

Pattern formation in two-dimensional square-shoulder systems

Julia Fornleitner^{1,2} and Gerhard Kahl²

¹ Institut für Festkörperforschung, Forschungszentrum Jülich, D-52425 Jülich, Germany

² Institut für Theoretische Physik and Centre for Computational Materials Science (CMS), Technische Universität Wien, Wiedner Hauptstraße 8-10, A-1040 Wien, Austria

E-mail: fornleitner@cmt.tuwien.ac.at

Received 25 September 2009

Published 23 February 2010

Online at stacks.iop.org/JPhysCM/22/104118

Abstract

Using a highly efficient and reliable optimization tool that is based on ideas of genetic algorithms, we have systematically studied the pattern formation of the two-dimensional square-shoulder system. An overwhelming wealth of complex ordered equilibrium structures emerge from this investigation as we vary the shoulder width. With increasing pressure three structural archetypes could be identified: cluster lattices, where clusters of particles occupy the sites of distorted hexagonal lattices, lane formation, and compact particle arrangements with high coordination numbers. The internal complexity of these structures increases with increasing shoulder width.

1. Introduction

The so-called core-softened systems, introduced by Hemmer and Stell [1], are characterized by a potential with an impenetrable core region and an adjacent, repulsive potential tail of variable shape. Over many years it was commonly believed that these systems are not able to self-organize in ordered structures other than trivial, close-packed lattices, due to the radial symmetry of the potential and due to the complete absence of attraction. Thus, it was even more surprising that investigations, carried out essentially during the past decade, revealed a completely different scenario: particles interacting via core-softened potentials *are* able to self-organize in a surprisingly rich wealth of ordered equilibrium structures. The first systematic studies on two-dimensional core-softened potentials were pioneered by Jagla [2, 3]: using Monte Carlo simulations the author was able to provide evidence that—depending on the shape of the corona and on the system parameters—core-softened systems are able to display a rich wealth of ordered structures *beyond* the simple hexagonal lattice. Moreover, Jagla was able to show that these structures emerge not only at zero temperature, but also ‘survive’ at finite temperature. In the phase diagrams presented in [3] patterns emerge, that distinctively differ from the hexagonal lattice with its six nearest neighbours (n_b): lanes or lamellae ($n_b = 2$), ring-like structures ($n_b = 3$), or compact structures ($n_b = 4$) other than the hexagonal lattice. In

later work [4, 5], an additional cluster phase was identified for the square-shoulder system. These simulation-based investigations were complemented with a mean-field theory proposed by Glaser *et al* [6], based on which ‘a remarkable array of aggregate phases arising from the competition between the hard core and soft shoulder length scales, including fluid and crystalline phases with micellar, lamellar, and inverse micellar morphology’ were identified. A closely related contribution was published recently [7].

The aim of the present article is to contribute to a deeper and comprehensive understanding of how particles, interacting via core-softened potentials, self-assemble in ordered equilibrium structures. We have restricted our contribution to the square-shoulder system for the following reason: due to its simple functional form, the internal energy of the system, U , can be calculated directly by counting the number of overlapping coronas in a given ordered particle arrangement, guaranteeing thus the highest numerical accuracy possible for the evaluation of the lattice sum. This particular feature has turned out to be very helpful in reliably identifying all possible self-assembly scenarios of the system. A preliminary account of these investigations has already been given in [8].

The identification of ordered equilibrium structures can be cast into an optimization problem: following basic laws of thermodynamics, particles will arrange in such a way that the related thermodynamic potential is minimized. In an

effort to solve this highly non-trivial optimization problem we have used a numerical tool based on ideas of genetic algorithms (GAs) [9]. In this approach possible ordered particle arrangements are considered as individuals that are exposed to an artificial evolution on the computer. The individuals have to survive under the condition that the thermodynamic potential of the structure associated with the individuals is minimized. Working in the NPT ensemble, the relevant thermodynamic potential is the Gibbs free energy, G . Numerous applications of this optimization tool to identify ordered equilibrium structures in soft matter systems have provided evidence that the approach is efficient, reliable, and copes extremely well with high dimensional search spaces and rugged energy landscapes [8, 10–25]. Our investigations are restricted to $T = 0$; thus any approximate feature introduced via the entropic contribution is excluded *a priori*. This assumption in combination with the extremely high success rate of GA-based optimization tools make us confident that we were able to identify all possible minimum energy configurations (MECs) of the system.

In our investigations we have found a surprisingly rich wealth of structures. These results can be summarized as follows: (i) an increasing pressure induces a transition from cluster lattices to lanes and then to highly coordinated compact structures; (ii) the complexity of the cluster structures and lanes increases with growing shoulder width, λ . The reasons why this simple, spherically symmetric potential is able to induce a rich variety of ordered structures, which are often characterized by strongly asymmetric particle arrangements, is not obvious at first sight. However, as we will give evidence for in the present contribution, the formation of these structures can be traced back to the competition of two length scales, the diameter of the hard core, σ , and the range of the shoulder, $\lambda\sigma$, and to simple energetic arguments [6].

The paper is organized as follows. In the next section we briefly present the model and give a short account of our GA-based optimization technique. Section 3 is dedicated to the results and the paper is closed with concluding remarks.

2. Model and theoretical tools

2.1. Model

In a square-shoulder system, hard particles of diameter σ interact via a soft, repulsive, step-shaped corona of width $\lambda\sigma$ and height $\epsilon(>0)$. The spherically symmetric pair potential $\Phi(r)$ for this system reads as

$$\Phi(r) = \begin{cases} \infty & r < \sigma \\ \epsilon & \sigma \leq r < \lambda\sigma \\ 0 & \lambda\sigma \leq r. \end{cases} \quad (1)$$

We choose σ and ϵ as the length and energy scales. The system is further characterized by an (area) number density $\eta = N/A$, N being the number of particles per unit cell and A being the area of the unit cell.

The square-shoulder system with its repulsive corona is typical for steric interactions and is therefore often used to

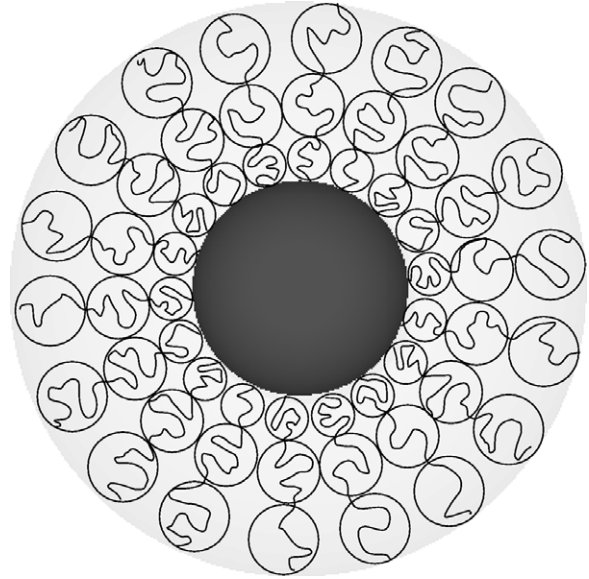


Figure 1. Schematic representation of a polymer-grafted colloid. Dark—core region, grey-shaded region—polymer corona.

model the behaviour of particles that exhibit a distinct core-corona architecture, such as polymer-grafted colloids [26]: the colloids themselves are impenetrable, thus forming the hard core; the soft coronas, on the other hand, that consist of the polymer chains, can interpenetrate at some energy cost, leading to the soft, repulsive, step-shaped shoulder in the pair potential adjacent to the hard core region. The potential parameters, ϵ and σ , can be controlled by changes in the grafting density and in the length of the polymer chains, respectively (see figure 1). Other examples of particles whose pair interaction has been modelled using the square-shoulder potentials are micelles of dendritic polymers [27] and diblock copolymers [28, 29]. The micelles formed by these two kinds of polymers display two distinct regions: the inner core, composed of the solvophobic parts of the constituent polymers, is characterized by a high polymer density, whereas the solvophilic polymer groups form a diffuse corona that is considerably less dense and thus interpenetrable, leading to the characteristic inner architecture.

Working in the NPT ensemble, the relevant thermodynamic potential is the Gibbs free energy, $G = U - ST + PA$. Assuming, in addition, a vanishing temperature, G becomes

$$G = U + PA. \quad (2)$$

Thus, the evaluation of the thermodynamic potential reduces essentially to the evaluation of the lattice sum, U . In view of the simple functional form of the square-shoulder potential (1), U can be simply determined by counting the overlapping coronas for a given ordered particle configuration.

We have introduced the following reduced thermodynamic quantities: $P^* = P\sigma^2/\epsilon$, $U^* = U/(N\epsilon)$, and $G^* = G/(N\epsilon) = U^* + P^*/(\eta\sigma^2)$. U_{\max}^* will denote the maximal internal energy obtained for a given shoulder width. As outlined below, this simple dependence on η of G^* considerably facilitates the search for ordered equilibrium structures.

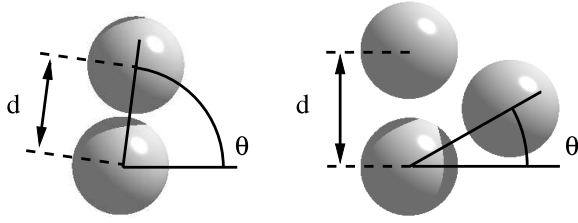


Figure 2. Schematic representation of dimers and trimers populating the lattice sites of a cluster lattice (see the text). The two additional parameters for describing the clusters, d and θ , are indicated for a dimer (left) and a trimer (right).

2.2. Theoretical tools

To identify the MECs of our system we have used the genotype implementation of the GA-based search strategy presented in more detail in [30] and suitably adapted to the two-dimensional case. As an additional feature we have introduced a ‘cluster-biased’ search strategy. We assume that the sites of the lattice are populated by regular dimers or trimers, each of them parametrized by internal parameters (cf figure 2) which characterize the orientation of the clusters and the relative distances of the particles within the cluster. In this way, we were able to considerably increase the number of particles within the unit cell to 15 particles and concomitantly enhance the performance of the search strategy when dealing with complex lattices. The fact that the search algorithm proposes unphysical lattices with overlapping core regions does not affect the numerical performance to a comparable extent to in the three-dimensional case [15, 16, 31]. It was therefore sufficient to implement the hard core exclusion in the parametrization of the primitive lattice only and rule out lattices with overlapping basis particles in the evolutionary process later on. For the fitness function which characterizes the quality of an individual \mathcal{I} , which represents a possible candidate structure, we have used the canonical form, i.e.,

$$f(\mathcal{I}) = \exp\{-[G(\mathcal{I}) - G(\mathcal{I}_0)]/G(\mathcal{I}_0)\}. \quad (3)$$

\mathcal{I}_0 represents some reference structure. Working in the NPT ensemble, the number density η has to be encoded in the individual \mathcal{I} : applying the external pressure P for a given state point, the search algorithm then provides the optimized lattice and η as output.

3. Results

The special form of the interaction potential (1) leads to a characteristic functional dependence of U^* and G^* on P^* : each structure is characterized by its number of corona overlaps, so the internal energy U^* of this structure has a fixed rational value, given by the number of corona overlaps per particle. As long as the structure does not change, the internal energy is the same, irrespective of the applied pressure. The corresponding Gibbs free energy $G^* = G^*(P^*)$ of a single structure is therefore given by a straight line of slope $1/\eta$ in a (G^*, P^*) -diagram. In this context we can identify

two limiting structures, which occur for all values of λ : at very low pressure, the system will arrange so that discs of diameter λ form a hexagonally close-packed structure. As no overlaps of coronas occur in this configuration, the internal energy vanishes, $U_{\text{low}}^* = 0$, and we obtain

$$\eta_{\text{low}} = \frac{2}{\sqrt{3}(\lambda\sigma)^2}. \quad (4)$$

The configuration of maximal internal energy and density is encountered at high pressure values and is given by another hexagonally close-packed structure, where the hard core of each particle is in direct contact with its six nearest neighbours. The internal energy thus reaches its maximal value, $U_{\text{high}}^* = U_{\text{max}}^*(\lambda)$, and the number density of this incompressible structure can be written as

$$\eta_{\text{high}} = \frac{2}{\sqrt{3}\sigma^2}. \quad (5)$$

As η_{low} and η_{high} are the minimal and maximal values of the number density, all other MECs for a given shoulder width λ have to be located on straight lines of slope $1/\eta$ in a (G^*, P^*) -diagram, with

$$\frac{1}{\eta_{\text{high}}} \leq \frac{1}{\eta} \leq \frac{1}{\eta_{\text{low}}}. \quad (6)$$

On the basis of this particular feature we have used an efficient algorithm [15, 32] for a systematic scan along the pressure axis: we first determine the pressure value which corresponds to the intersection point of the two lines representing the above discussed limiting cases in the (G^*, P^*) -diagram. For this pressure value, a GA is then employed, leading to a configuration of lower Gibbs free energy. This Gibbs free energy of the newly found structure is again represented by a straight line as a function of pressure which we intersected with the previous lines, yielding two new pressure values. At these values, GA runs are again performed. By iterating this procedure, we are able to investigate the whole pressure regime in a highly efficient way, without risking missing a MEC due to an inappropriately spaced pressure grid. In the end, the Gibbs free energy $G^* = G^*(P^*)$ appears as a sequence of intersecting straight lines over the entire pressure range.

In the following, we will discuss the general trends in structure formation, showing representative examples of the structures proposed by the GA. The complete sequences of MECs for all values of shoulder width $\lambda\sigma$ investigated can be found in [33].

3.1. Shoulder width $\lambda = 1.5\sigma$

We start our survey at a shoulder width of $\lambda = 1.5\sigma$ and show the MECs proposed by the GA in figure 3: at very low pressure, the particles are found to form an ideal hexagonal lattice, avoiding overlapping coronas. Upon compression, the system must ‘pay a tribute’ to the reduced space in terms of an energy penalty, i. e. via a first overlap of shoulders, and lane formation emerges as an energetically convenient solution. Along the lanes, particles are in direct contact, forming a one-dimensional close-packed arrangement. Parallel lanes try to

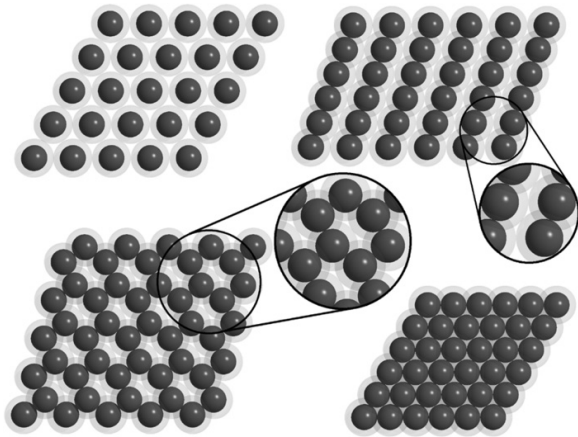


Figure 3. Complete sequence of MECs for the square-shoulder system of shoulder range $\lambda = 1.5\sigma$. Dark spheres mark the particles' hard cores, whereas the repulsive shoulders are depicted as grey coronas. Configurations correspond (from left to right and from top to bottom) to pressure values indicated in figure 4 by vertical arrows.

avoid corona overlap and the shoulder width λ serves as a spacer (see the magnified view in figure 3). As the pressure is further increased, new strategies are required to arrange particles in an energetically favourable way. While particles still prefer alignment along lanes, the internal arrangement is modified: rather than forming straight lines, the lanes are now zigzag shaped, which is a trade-off between the reduced available space and the energetic penalty due to additional corona overlaps. Neighbouring lanes are arranged such that each particle is now in direct contact with three others (see the magnified view in figure 3). These staggered lanes can also be viewed as ring-like structures where six particles form elongated rings with λ fixing the width of the cage. Further compression causes the system to collapse into the hexagonally close-packed structure, where each particle is in direct contact with its six nearest neighbours.

Figure 4 displays the corresponding thermodynamic properties $G^* = G^*(P^*)$ and $U^* = U^*(P^*)$, where the characteristic features of the two thermodynamic quantities mentioned above are clearly visible: the internal energy appears as a distinct sequence of flat plateaus, each representing one of the identified MECs, whereas the individual line segments, which contribute to the Gibbs free energy over the entire pressure range, are also easily recognized in the (G^*, P^*) -diagram.

3.2. Shoulder width $\lambda = 3\sigma$

As we proceed to a shoulder width of $\lambda = 3\sigma$, the system develops completely different strategies to form MECs as the pressure is increased, leading to a considerably broader variety of different structures compared to the case $\lambda = 1.5\sigma$. The selection of configurations shown in figure 5 captures the general trends in the MECs identified; the corresponding thermodynamic properties are displayed in figure 6.

The hexagonal pattern imposed by the non-overlapping coronas, which is observed for very low pressure values only

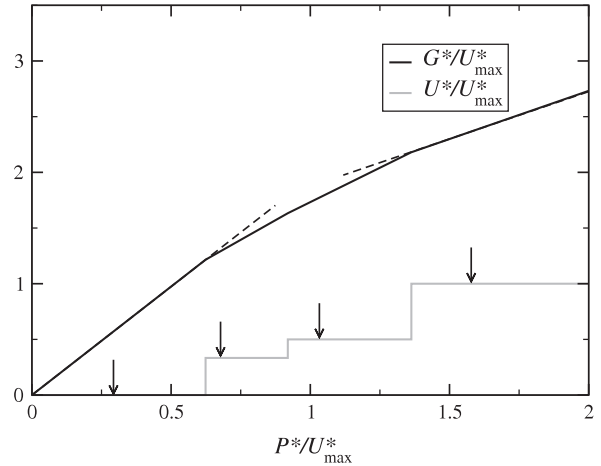


Figure 4. Gibbs free energy (black line), G^* , and internal energy (grey line), U^* , as functions of P^* for a system of shoulder range $\lambda = 1.5\sigma$, all scaled with $U_m^* = 3$, the internal energy of the hexagonally close-packed structure. Vertical arrows indicate MECs depicted in figure 3. Broken lines indicate limiting cases of MECs (see the text).

and not displayed in figure 5, is soon superseded by a novel strategy, namely the formation of clusters. At low pressure, dimer and trimer clusters are found to form distorted hexagonal lattices, where the degree of deviation from the ideal structure is imposed by the shape of the clusters. In this way, the dimers form a strongly distorted hexagonal lattice, whereas the trimers sit on an almost ideal hexagonal structure: in the trimer lattice, the angle ϕ between the two lattice vectors amounts to $\phi_{\text{trimer}} = 60.8^\circ$, whereas in the dimer lattice the angle ϕ_{dimer} deviates strongly from the ideal value of the hexagonal structure, with $\phi_{\text{dimer}} = 65^\circ$, and also the lattice vectors differ distinctly in size in the dimer case.

As the system is further compressed the formation of clusters becomes energetically less attractive and lane formation sets in. In the beginning, each lane is built up by a single, linear chain of particles, resembling the first lane scenario encountered for $\lambda = 1.5\sigma$, but for increasing pressure, the internal architecture of the lanes gets more complex: besides the lanes formed by single chains of particles mentioned above, we observe a dense dimer phase, that can easily be interpreted as a lane-like scenario, a striped phase of double chains and pearl-necklace structures. As the pressure is increased further, the system collapses to close-packed structures characterized by a compact distribution of particles, until the high pressure limit of an hexagonally close-packed lattice is finally reached, where the hard core of each particle is in direct contact with its six nearest neighbours.

This considerably richer wealth of MECs encountered for $\lambda = 3\sigma$ is reflected by the increased number of energy levels in the plot U^* versus P^* and the larger number of intersecting straight line segments in the (G^*, P^*) -diagram in figure 6.

3.3. Shoulder width $\lambda = 5\sigma$

For $\lambda = 5\sigma$, the general trends already observed in the previous cases of $\lambda = 1.5\sigma$ and 3σ get more pronounced

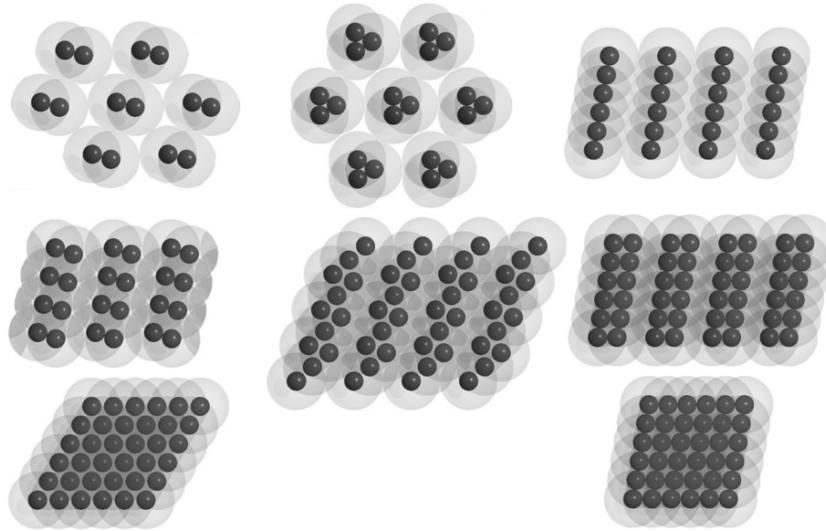


Figure 5. Selection of MECs for the square-shoulder system of shoulder range $\lambda = 3\sigma$. Dark spheres mark the particles' hard cores, whereas the repulsive shoulders are depicted as grey coronas. Configurations correspond (from left to right and from top to bottom) to pressure values indicated in figure 6 by vertical arrows.

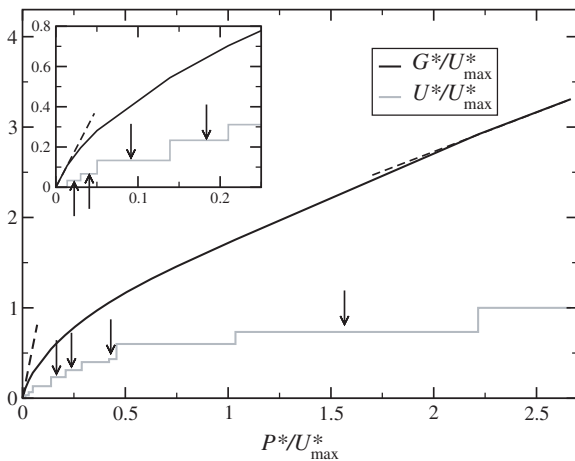


Figure 6. Gibbs free energy (black line), G^* , and internal energy (grey line), U^* , as functions of P^* for a system of shoulder range $\lambda = 3\sigma$, all scaled with $U_m^* = 15$, the internal energy of the hexagonally close-packed structure. Vertical arrows indicate MECs depicted in figure 5. Broken lines indicate limiting cases of MECs (see the text).

(see figure 7). Again, the structures presented in figure 7 are a representative selection from the complete sequence of MECs found for $\lambda = 5\sigma$. Figure 8 displays $G^* = G^*(P^*)$ and $U^* = U^*(P^*)$.

The low pressure regime is populated by clusters, arranged on an underlying distorted hexagonal lattice. As the pressure increases, those aggregates become larger until they reach a size of four particles. Upon further compression, the system again prefers to form lane-like structures of various shapes: we observe striped phases with up to four particles per lane as well as parallel zigzag-shaped lanes. The increasing complexity of the inner structure of the lanes makes simple energetic explanations in terms of overlapping coronas hard to perceive, but the magnified views in figure 7 give evidence that the

formation of the different lane structures is an efficient strategy for avoiding an overlap between the coronas of particles belonging to neighbouring lanes. In addition, we encounter a phenomenon that can be interpreted as a first observation of a narrow crossover region from cluster-populated lattices to striped phases: first single particles, then dimers, arrange in a lane-like configuration, but without the particles being in hard core contact along the lane. Above a certain pressure threshold, the formation of lanes is no longer energetically favourable and the system collapses to close-packed configurations with a compact distribution of particles, like the square lattice shown in figure 7.

3.4. Shoulder width $\lambda = 7\sigma$

The complexity of internal arrangements increases further in all three kinds of structures encountered—clusters, lanes and close-packed arrangements—as the shoulder width changes to $\lambda = 7\sigma$. Figure 9 shows a representative collection of the already considerably large number of MECs proposed by the GA; $U^* = U^*(P^*)$ and $G^* = G^*(P^*)$ are displayed in figure 10.

Starting from the low density hexagonally close-packed structure, which is not depicted in figure 9, we observe clusters of growing size for increasing pressure: the dimers shown in figure 9 are soon superseded by trimers, and later by clusters consisting of four, six, or even eight particles. The eight-particle clusters are of an almost circular shape as can be seen in the magnified view in figure 9 and thus allow for an arrangement very close to the energetically favoured hexagonal configuration. Although the eight-particle cluster structure was found to be stable over a comparatively large range of pressure values (see figure 10), we have to note, however, that the occurrence of this particular cluster size is possibly due to the chosen parametrization of lattices: the cluster-biased parametrization as presented in section 2.2 favours

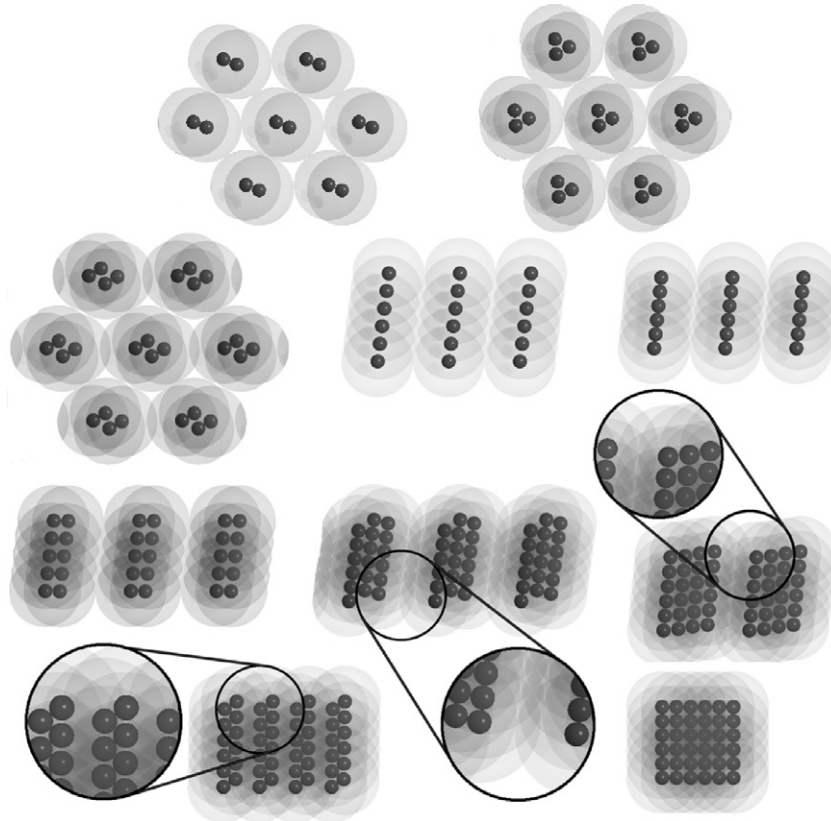


Figure 7. Selected MECs for the square-shoulder system of shoulder range $\lambda = 5\sigma$. Dark spheres mark the particles’ hard cores, whereas the repulsive shoulders are depicted as grey coronas. Configurations correspond (from left to right and from top to bottom) to pressure values indicated in figure 8 by vertical arrows.

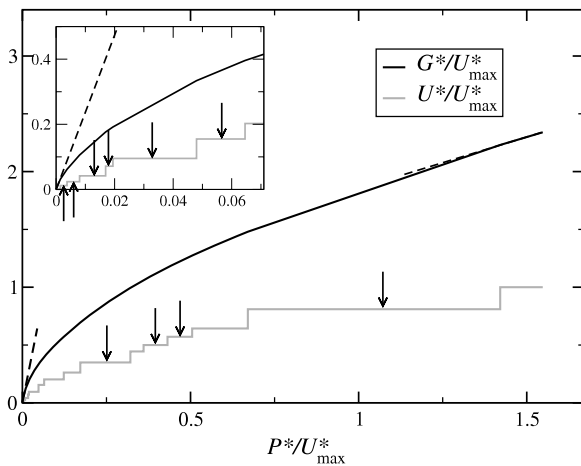


Figure 8. Gibbs free energy (black line), G^* , and internal energy (grey line), U^* , as functions of P^* for a system of shoulder range $\lambda = 5\sigma$, all scaled with $U_m^* = 42$, the internal energy of the hexagonally close-packed structure. Vertical arrows indicate MECs depicted in figure 7. Broken lines indicate limiting cases of MECs (see the text).

the formation of clusters consisting of six or eight particles, whereas clusters of seven particles, which allow for aggregates even closer to the preferred circular shape, are not available

to the cluster-biased parametrization and can enter the survey only via calculations employing the standard description of two-dimensional lattices.

Like the cluster phases, the lane-like structures also increase in complexity as the shoulder width reaches the value $\lambda = 7\sigma$: arrangements of lanes that are two, three, four and six particles wide are found in the intermediate pressure regime, displaying a broad variety in their internal architecture. Surprisingly, structures consisting of single-particle chains fail to show up completely among the discovered MECs [33].

Furthermore, we can now distinguish two different crossover regions for systems of shoulder width $\lambda = 7\sigma$: first, a regime of crossover from the clustered phases to the lane-like scenarios similar to the one observed for systems with $\lambda = 5\sigma$, where dimers arrange in lanes with the inter-dimer distance within one lane gradually decreasing as more pressure is applied to the system. Second, we observe a crossover from lane-like structures to the close-packed configurations encountered at high pressure values, as compact particle distributions are found to alternate with phases exhibiting distinct stripes.

3.5. Shoulder width $\lambda = 10\sigma$

Finally, for $\lambda = 10\sigma$, the largest shoulder width investigated, the strategies of the system for arranging particles in

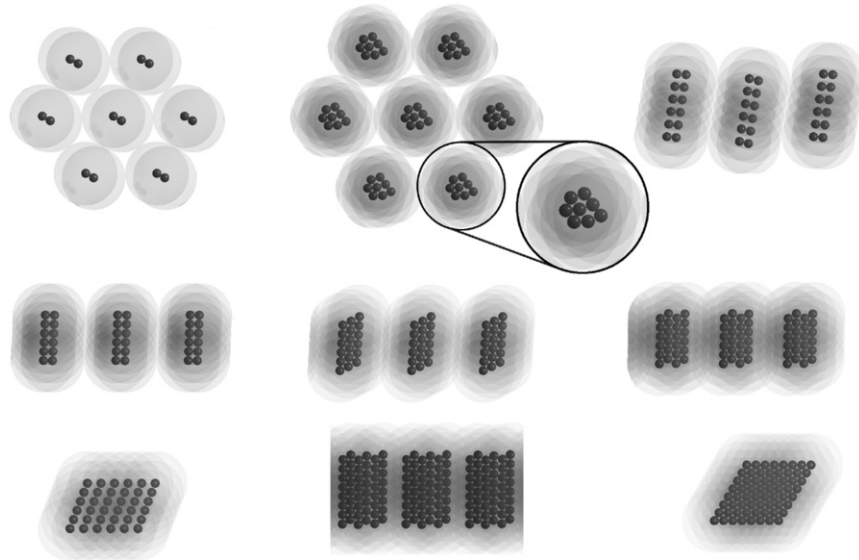


Figure 9. Selected MECs for the square-shoulder system of shoulder range $\lambda = 7\sigma$. Dark spheres mark the particles' hard cores, whereas the repulsive shoulders are depicted as grey coronas. Configurations correspond (from left to right and from top to bottom) to pressure values indicated in figure 10 by vertical arrows.

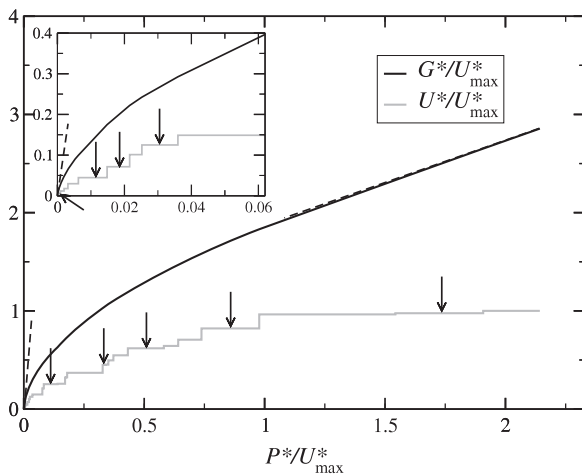


Figure 10. Gibbs free energy (black line), G^* , and internal energy (grey line), U^* , as functions of P^* for a system of shoulder range $\lambda = 7\sigma$, all scaled with $U_m^* = 84$, the internal energy of the hexagonally close-packed structure. Vertical arrows indicate MECs depicted in figure 9. Broken lines indicate limiting cases of MECs (see the text).

energetically favourable configurations seem to be similar to the previous cases at first sight: the hexagonal pattern of minimum density, which is not included in the selection of MECs shown in figure 11, is soon replaced as the system prefers the formation of clustered lattices. The formation of lanes of increasingly complex inner structure is preferred at intermediate and high pressure values, and the crossover regions, first from cluster-shaped particle arrangements to lane-like structures and second from lanes to the close-packed regime, are both visible and more pronounced, than in the previous cases.

The differences between the MECs of the comparatively large shoulder length of $\lambda = 10\sigma$ and those obtained for the intermediate values discussed above are of subtle nature and concern the internal arrangement of particles in the structures: although the growing cluster arrangements are located on slightly distorted hexagonal lattices like in the previous cases, the system's strategy for forming MECs has changed, as we observe that inside a cluster the cores of the particles sometimes arrange in a disordered fashion (see the magnified views in figure 11), while for intermediate values of λ only clusters with an ordered internal particle arrangement occur. The reason for this change is obviously the following: as soon as λ is sufficiently large to support cluster formation, the system tries to arrange particles in clusters shaped as circularly as possible, leading to an underlying structure as close as possible to the energetically favourable hexagonal lattice. For intermediate shoulder widths, the core region still represents a considerable fraction of the particle diameter, so ordered arrangements of particles are necessary for building clusters as circular in shape as possible. For $\lambda = 10\sigma$, however, the core region is nearly negligible with respect to the corona width, so both regular and irregular particle arrangements inside the cluster can lead to circular-shaped aggregates of the same size, thus having practically the same value of G (see figure 12).

4. Conclusion

In this contribution we have reported about the rich wealth of ordered equilibrium structures in the two-dimensional square-shoulder system which we were able to identify by systematically varying the shoulder width and pressure. In view of the high success rate of the optimization tool that we have used to find these structures and due to the simple analytic

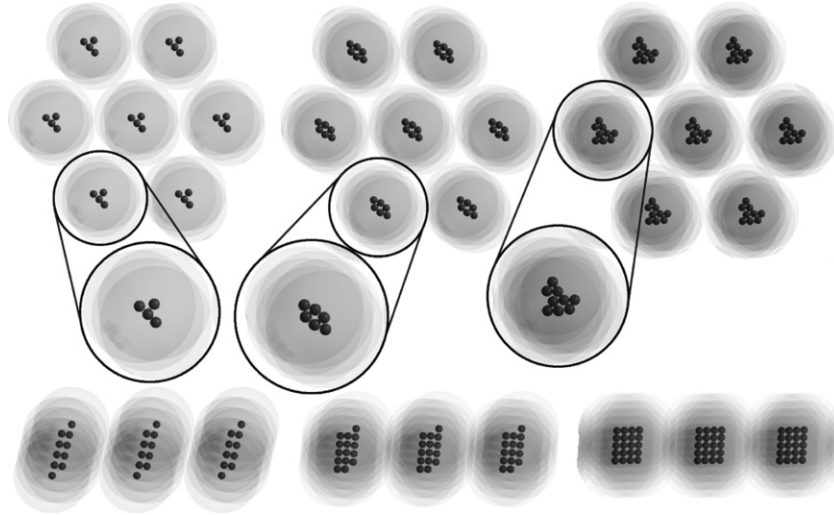


Figure 11. Selected MECs for the square-shoulder system of shoulder range $\lambda = 10\sigma$. Dark spheres mark the particles' hard cores, whereas the repulsive shoulders are depicted as grey coronas. Configurations correspond (from left to right and from top to bottom) to pressure values indicated in figure 12 by vertical arrows.

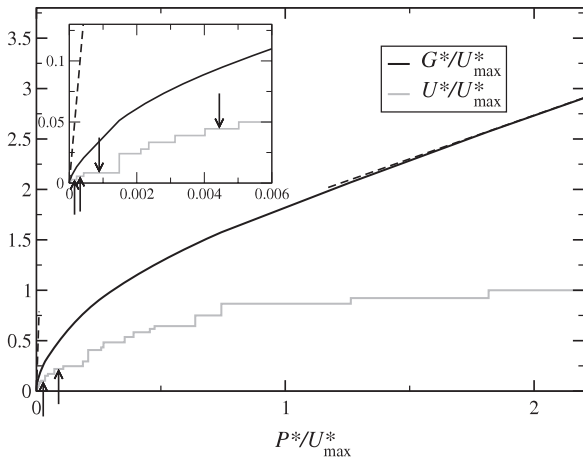


Figure 12. Gibbs free energy (black line), G^* , and internal energy (grey line), U^* , as functions of P^* for a system of shoulder range $\lambda = 10\sigma$, all scaled with $U_m^* = 180$, the internal energy of the hexagonally close-packed structure. Vertical arrows indicate MECs depicted in figure 11. Broken lines indicate limiting cases of MECs (see the text).

form of the pair interaction, we are confident that the sequences of MECs that we were able to identify are complete.

The observed trends in structure formation can be nicely summarized in a schematic diagram, depicted in figure 13. It displays the MECs identified as functions of the two relevant parameters, i.e., pressure and shoulder width. At low pressure the system forms cluster lattices. Here clusters of particles with overlapping corona occupy the sites of a regular or distorted hexagonal lattice. In an effort to minimize the Gibbs free energy the system tries to form circular-shaped clusters. Thus, the envelope of all coronas of a given cluster defines essentially the spacer between lattice sites in the underlying lattice. As we increase the pressure, these clusters

rearrange and henceforward form lanes. The internal shape of these lanes is dictated by a trade-off between the corona overlaps within the lanes and the corona overlap between neighbouring lanes. Again, the shoulder width represents essentially the spacer between isolated neighbouring lanes or sets of lanes. Finally, at the highest available pressure, particles form compact structures with high coordination numbers, i.e., with four or six neighbouring particles. Among these ordered structures are the four-coordinated oblique and square lattices, and, of course, the six-coordinated hexagonal lattice. As we move along the orthogonal direction in the schematic diagram (cf figure 13), we observe an increasing complexity in the internal structure of the building blocks of the aforementioned structural archetypes, i.e. the clusters and lanes, as the range of the shoulder becomes wider. This increasing degree of disorder is a precursor of the behaviour known from a number of closely related systems, that have been studied in the three-dimensional case: the penetrable sphere model [34, 35], which represents the limiting case $\lambda \rightarrow \infty$ of our square-shoulder system, and the generalized exponential model [13, 14, 36]. In both cases, disordered clusters of overlapping particles were found to arrange on the sites of regular lattices.

We point out that a similar trend of structural archetypes has been observed for the three-dimensional square-shoulder system [15, 16]. Here, four structural archetypes are encountered as the pressure increases: first, the cluster phases, followed by the columnar and lamellar structures (which in the two-dimensional case reduce to the archetype of lane formation), and, finally, the compact structures. Again, as we increase the range of the shoulder, the internal complexity grows. This relates also to the underlying structure: the clusters now occupy a considerably richer wealth of three-dimensional lattices (such as fcc, bcc, and triclinic) and for the compact structures cover a broad range of structures (such as fcc, hcp, body centred orthogonal, and centred tetragonal), with a considerably larger range of nearest neighbours.

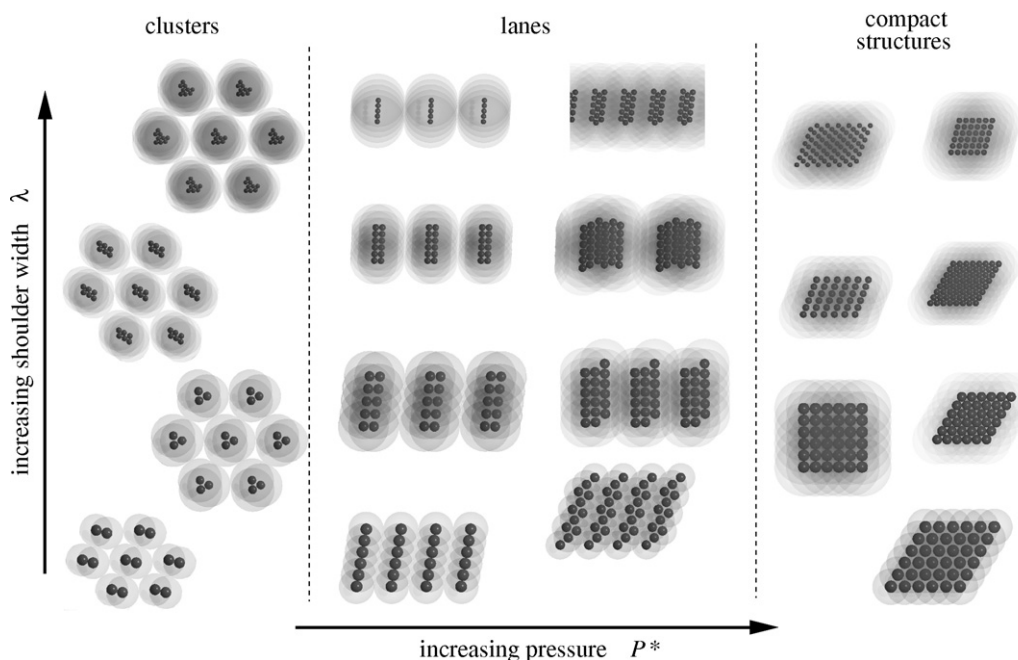


Figure 13. Schematic diagram of MECs encountered in the square-shoulder system as pressure P and shoulder width λ are varied.

Acknowledgments

The authors are indebted to Dieter Gottwald and Gernot J Pauschenwein (both of Vienna) for stimulating discussions and for computational aid. Financial support by the Austrian Science Foundation (FWF) under Projects Nos P17823-N08 and P19890-N16 is gratefully acknowledged.

References

- [1] Hemmer P C and Stell G 1970 *Phys. Rev. Lett.* **24** 1284–7
- [2] Jagla E 1998 *Phys. Rev. E* **58** 1478
- [3] Jagla E 1999 *J. Chem. Phys.* **110** 451
- [4] Malescio G and Pellicane G 2003 *Nat. Mater.* **2** 97
- [5] Malescio G and Pellicane G 2004 *Phys. Rev. E* **70** 021202
- [6] Glaser M, Grason G M, Kamien R, Košmrlj A, Santangelo C D and Zihnerl P 2007 *Europhys. Lett.* **78** 46004
- [7] Shin H, Grason G M and Santangelo C D 2009 *Soft Matter* **5** 3629
- [8] Fornleitner J and Kahl G 2008 *Europhys. Lett.* **82** 18001
- [9] Holland J 1975 *Adaptation in Natural and Artificial Systems* (Ann Arbor: The University of Michigan Press)
- [10] Stucke D P and Crespi V H 2003 *Nano Lett.* **3** 1183
- [11] Gottwald D, Likos C N, Kahl G and Löwen H 2004 *Phys. Rev. Lett.* **92** 068301
- [12] Gottwald D, Likos C N, Kahl G and Löwen H 2005 *J. Chem. Phys.* **122** 074903
- [13] Mladek B M, Gottwald D, Kahl G, Neumann M and Likos C N 2006 *Phys. Rev. Lett.* **96** 045701
Mladek B M, Gottwald D, Kahl G, Neumann M and Likos C N 2006 *Phys. Rev. Lett.* **97** 019901
- [14] Likos C N, Mladek B M, Gottwald D and Kahl G 2007 *J. Chem. Phys.* **126** 224502
- [15] Pauschenwein G J and Kahl G 2008 *Soft Matter* **4** 1396–9
- [16] Pauschenwein G J and Kahl G 2008 *J. Chem. Phys.* **129** 174107
- [17] Fornleitner J, Lo Verso F, Kahl G and Likos C N 2008 *Soft Matter* **4** 480
- [18] Dobnikar J, Fornleitner J and Kahl G 2008 *J. Phys.: Condens. Matter* **20** 494220
- [19] Fillion L and Dijkstra M 2009 *Phys. Rev. E* **79** 046714
- [20] Tüchtmantel T, LoVerso F and Likos C N 2009 *Mol. Phys.* **107** 523
- [21] Chremos A and Likos C N 2009 *J. Phys. Chem. B* **113** 12316
- [22] Kahn M, Weis J-J, Likos C N and Kahl G 2009 *Soft Matter* **5** 2852
- [23] Fornleitner J, LoVerso F, Kahl G and Likos C N 2009 *Langmuir* **25** 7836
- [24] Nikoubashman A and Likos C N 2010 *J. Phys.: Condens. Matter* **22** 104107
- [25] Doppelbauer G, Bianchi E and Kahl G 2010 *J. Phys.: Condens. Matter* **22** 104105
- [26] Norizoe Y and Kawakatsu T 2005 *Europhys. Lett.* **72** 583
- [27] Balagurusamy V S K, Ungar G, Perc V and Johansson G 1997 *J. Am. Chem. Soc.* **119** 1539
- [28] McConnell G A and Gast A P 1996 *Phys. Rev. E* **54** 5447
- [29] McConnell G A and Gast A P 1997 *Macromolecules* **30** 435
- [30] Gottwald D, Kahl G and Likos C N 2005 *J. Chem. Phys.* **122** 204503
- [31] Pauschenwein G J 2009 *J. Phys. A: Math. Theor.* **42** 355204
- [32] Pauschenwein G J 2008 *PhD Thesis* Institut für Theoretische Physik, TU Wien available at: <http://tph.tuwien.ac.at/smt/extra/publications/phd/pauschenwein.pdf>
- [33] Fornleitner J 2008 *PhD Thesis* Institut für Theoretische Physik, TU Wien available at: <http://tph.tuwien.ac.at/smt/extra/publications/phd/fornleitner.pdf>
- [34] Likos C N, Watzlawek M and Löwen H 1998 *Phys. Rev. E* **58** 3135
- [35] Mladek B, Falkinger G and Kahl G 2008 unpublished
- [36] Mladek B M, Gottwald D, Kahl G, Neumann M and Likos C N 2008 *J. Phys. Chem. B* **111** 12799–808